Int. J. Metrol. Qual. Eng. **13**, 11 (2022)

https://doi.org/10.1051/ijmqe/2022013

International Journal of Metrology and Quality Engineering

Available online at:
www.metrology-journal.org

RESEARCH ARTICLE OPEN ACCESS

Series arc fault identification based on complete ensemble empirical mode decomposition with adaptive noise and convolutional neural network

Tongtong Shang[1], Wei Wang[1,*], Jigang Peng[2], Bingyin Xu[1], Haiyang Gao[1], and Guoliang Zhai[1]

[1]School of Electrical and Electronic Engineering, Shandong University of Technology, Zibo 255000, PR China
[2]Shandong Electronic Information Products Inspection Institute (China Saibao (Shandong) Laboratory), Jinan 250014, PR China

Received: 24 June 2022 / Accepted: 24 September 2022

Abstract. The effective identification of series arc faults is of considerable significance for preventing fires in residential buildings. Series arc fault currents and load currents have a similar waveform, and the fault features and nonfault features are superimposed on the current signal. Fault features are deeply hidden, making it difficult to identify them. This work proposes a method based on complete ensemble empirical mode decomposition with adaptive noise (CEEMDAN) preprocessing and a one-dimensional convolutional neural network (1DCNN). The CEEMDAN algorithm is used to decompose the collected current signals. Then, the intrinsic mode function (IMF) components with no representational significance are eliminated by calculating the Spearman correlation coefficient before inputting it into the 1DCNN. The experimental results showed that the accuracy of the method for the measured load is 99.3%. Compared with the method that directly uses original current signals as model inputs, the recognition accuracy of the algorithm was significantly improved. Therefore, the proposed algorithm can be used for series arc fault identification in residential building power distribution systems.

Keywords: Series arc / fault detection / CEEMDAN decomposition / one dimensional convolutional neural networks / characterization intrinsic mode function extraction

1 Introduction

An arc refers to the phenomena of luminescence and discharge, which are generated when the insulating medium between different electrodes occurs voltage breakdown. There are various reasons that lead to series arcs in distribution lines, such as loose contacts, aging insulation, rodent bites, and inappropriate wiring. The arc temperature generated by an electric current of 0.5 A can reach as high as 2000–3000 °C, and this temperature is enough to ignite any combustible material [1,2]. Note that arcs can occur with a maintenance voltage of as low as 20 V. Since series arc faults are connected with loads in series, usually, fault currents are slightly smaller than load currents. Moreover, it is difficult to distinguish the waveform characteristics of fault currents from those of nonlinear loads. Therefore, the accurate detection of series arc faults is of great significance with regard to the elimination of fire hazards.

The research on arc fault detection methods at home and abroad is divided into two categories. The first category entails detection based on physical characteristics, such as arc sound, arc light, and emitted heat after the generation of arcs [3–5], and it can only detect arc faults in a specific range, such as switchgear. The second category entails detection based on the fault characteristics of the line current and voltage. The detection method that uses fault current characteristics can monitor downstream lines by installing monitoring points upstream. Therefore, this method has become a research hotspot in the arc detection technology field. As for the detection methods based on fault current characteristics, the current detection methods primarily detect one or more characteristics of the time–frequency characteristics [6–8], zero-break characteristics [9], and high-frequency component characteristics [10,11] of fault current signals in the time domain or transformation domain. However, this method is subjective with regard to the selection of fault features and the setting of thresholds, which limits its feature expression ability of fault current signals to a certain extent. Thus, it is prone to misjudgment or omission. The artificial intelligence technology, which is represented by the neural network technology, is a new method for solving this problem, and relevant achievements have been made to date. Convolutional neural networks

* Corresponding author: wwsdut@163.com

(CNN) have powerful feature self-extraction capabilities, and can perceive the structural information of signals that traditional neural networks cannot perceive through convolutional layers. The structural information can significantly improve the recognition accuracy of the fully connected layer. The researchers in [12–14] took the raw current signal as a convolutional neural network input to identify series arc faults, thus verifying the feasibility of deep neural networks for arc fault detection. Because the fault information in original current signals is deeply hidden, it is not conducive to the feature extraction of convolution kernels. Yang et al. [15] proposed a method for preprocessing the raw current signal using a bandpass filter and took the filtered data as the input of CNN. Although the identifiable features were highlighted to certain extent, information from different frequency bands is still overlapping. Reference [16] proposed a method of using wavelet transform to preprocess original current signals and feed them to CNNs for training. Wavelet transform can only extract the components with fixed frequency bands, and different loads do not have common frequency bands with arc characteristics [17]. Thus, this method is not suitable for the fault diagnosis of specific loads.

As an adaptive decomposition method, empirical mode decomposition (EMD) does not require a preset basis function and can be adaptively decomposed into several IMF components as per the characteristics of input signals. Each IMF represents the original signal at different feature scales. Therefore, the EMD decomposition is especially suitable for the decomposition analysis of nonstationary nonlinear signals. CEEMDAN is a decomposition method that adds adaptive white noise to the EMD algorithm. Compared with the EMD method, this method improves the decomposition completeness and effectively reduces the effect of modal aliasing. Therefore, the CEEMDAN decomposition method is an effective tool for reflecting more essential fault current characteristics.

In view of the advantages of CEEMDAN in decomposing complex signals, a series arc fault identification method based on CEEMDAN and 1DCNN is proposed in this study. The method uses the CEEMDAN algorithm to realize the complete decomposition of original current signals. The characteristic IMF component is selected using the correlation coefficient, and the training set and test set are constructed using the characteristic IMF component. Finally, the series arc fault detection of the circuit is realized using 1DCNN. The test results demonstrated that the method can be effectively used in the series arc fault detection of low-voltage distribution lines.

2 Fault diagnosis model based on CEEMDAN-CNN

2.1 CEEMDAN theory and effective IMF extraction

In CNN diagnostic models, the quality of learning samples plays an important role with regard to accuracy. The current signal of a partial load has the characteristics of nonlinearity and nonstationarity, which are not conducive to the feature extraction of CNNs. Aiming to solving the poor quality problem of the learning samples composed of raw current signals, a signal preprocessing method based on CEEMDAN and a correlation analysis are herein proposed. The original signal can be decomposed into eigenmode function signals by the CEEMDAN algorithm, and its essential characteristics can be reflected more, which is extremely suitable for fault diagnosis.

The implementation steps of the CEEMDAN algorithm are as follows [18].

Define $x[n]$ as the original current signal, where $E_j(\cdot)$ is the jth-order IMF component obtained by decomposing the signal by the EMD method, ω_i is the white noise that is added for the i-th time and conforms to the standard normal distribution ($I = 1, 2, ..., I$), ε_k is the noise standard deviation ($k = 0, 1, ..., K$, K is the overall number of modes), and IMF_j is the jth-order IMF component obtained by the CEEMDAN decomposition.

– Use EMD to decompose the noised signal $x[n] + \varepsilon_0\omega_i[n]$ for I times and obtain the ensemble average value to obtain the first-order IMF component:

$$IMF_1[n] = \frac{1}{I}\sum_{i=1}^{I} E_1(x[n] + \varepsilon_0\omega_i[n]). \tag{1}$$

– Calculate the first-order residual signal:

$$r_1[n] = x[n] - IMF_1[n]. \tag{2}$$

– Add the noise component decomposed by EMD to the first-order residual signal $r_1[n]$ to obtain a new signal, namely, $r_1[n] + \varepsilon_1 \mathrm{E}_1(\omega_i[n])$. Repeat step (1) for this signal to get the second-order component:

$$IMF_2[n] = \frac{1}{I}\sum_{i=1}^{I} E_1(r_1[n] + \varepsilon_1 E_1(\omega_i[n])). \tag{3}$$

– For $k = 2, ..., K$, calculate the kth order residual:

$$r_k[n] = r_{k-1}[n] - IMF_k[n]. \tag{4}$$

– Add the noise component $\varepsilon_k E_k(\omega_i[n])$ to the kth order residual $r_k[n]$ to obtain a new signal, repeat step (1) for this signal, and obtain the $k+1$th order component as follows:

$$IMF_{k+1}[n] = \frac{1}{I}\sum_{i=1}^{I} E_1(r_k[n] + \varepsilon_k E_k(\omega_i[n])). \tag{5}$$

– Repeat steps (4) and (5) until the number of extreme points of the residual component does not exceed 2. Then, the decomposition is terminated, and the final residual component is

$$R[n] = x[n] - \sum_{k=1}^{K} IMF_k. \tag{6}$$

The original signal $x[n]$ can be expressed as follows:

$$x[n] = \sum_{k=1}^{K} IMF_k + R[n]. \tag{7}$$

Eliminating the components without fault features is helpful for improving the recognition rate of data-driven arc fault recognition models. After the original current signal is decomposed by CEEMDAN, multiple IMF components are obtained. Among the above-mentioned modal components, there are components without fault characteristics. If they are used as inputs of convolutional neural networks, they can cause the problems of large input data size, slow model convergence, and low accuracy. Since the fundamental frequency component exists in both normal and fault currents, the selection of the fundamental frequency component as a basis for choosing the characteristic IMF not only weakens the inherent influence of the power frequency component but also highlights the high-frequency fault characteristics of fault currents, thereby improving the correct identification rate.

The selection of the fundamental frequency component IMF is realized by calculating the Spearman correlation coefficient between each IMF component and standard power frequency sinusoidal current after CEEMDAN decomposition.

The frequency of the power–frequency alternating current is not a stable 50 Hz, and it fluctuates in a small range. Thus, the initial phase angle of each test object can be of any value. Therefore, it is necessary to perform phase alignment before calculating the Spearman correlation coefficient between the IMF component and standard power frequency sinusoidal currents. Considering that the power frequency component is still the main component before and after each load fault, the proposed method in this study uses the initial phase angle of the power frequency component as the initial phase angle of the raw current signal to achieve phase alignment. The process of phase alignment is as follows:

Obtain the frequency domain phasor of $i(n)$ in cycles:

$$a + bj = \{FFT[i(n)]\}_{50\text{Hz}}, \tag{8}$$

where a and b are the real and imaginary parts of the power frequency components of $i(n)$.

Calculate the initial phase angle θ of the power frequency component of $i(n)$:

$$\theta = arctan\left({}^{b}/_{a}\right). \tag{9}$$

Generate a standard power frequency sinusoidal current signal with an initial phase angle of θ.

The Spearman correlation coefficient [19] between the power frequency sinusoidal signal $I[n]$ and jth-order IMF component ρ_j is:

$$\rho_j = 1 - \frac{6\sum_{k=1}^{n}\left(I[n] - IMF_j[n]\right)}{n(n^2-1)}. \tag{10}$$

The absolute value of the correlation coefficient reflects the correlation between each modal component and the standard power frequency sinusoidal current. The larger the absolute value, the higher the degree of correlation between the two, and the smaller the absolute value, the lower the degree of correlation between the two. Compare the absolute values of the correlation coefficients of all the modal components, take the eight IMFs with the smallest absolute values of the correlation coefficient as effective components, and discard other modal components.

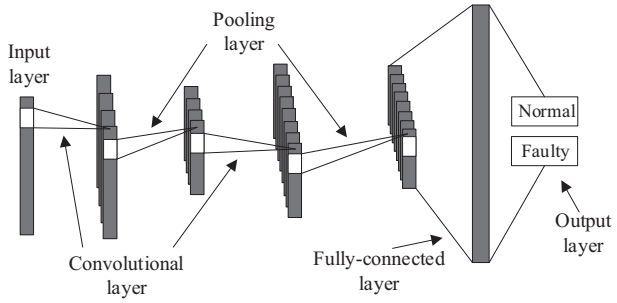

Fig. 1. Structure chart of CNN.

2.2 Fault diagnosis based on CNN

The fault diagnosis structure based on CNNs is shown in Figure 1 [20]. The convolutional neural network has three layers: input layer, hidden layer, and output layer. The hidden layer of the convolutional neural network includes three common constructions: convolutional layer, pooling layer, and fully connected layer. The input layer is one-dimensional data composed of effective IMF components concatenated together, and the form is as follows:

$$I_{input} = [IMF_1, IMF_2, L, IMF_8] \tag{11}$$

where IMF_k is the component obtained by CEEMDAN decomposition of raw current signal, k is the number of effective IMF components, $k = 1, 2, ..., 8$.

(1) Convolutional layer

The input data is mapped to the convolution layer after the convolution operation, as shown in formula (12). A rectified linear unit (ReLU), as shown in formula (13), is used as the activation function to alleviate the vanishing gradient issue. The ReLU is one of the most widely used activation functions when designing neural networks. A big advantage of the ReLU function compared to other activation functions is that it does not activate all neurons at the same time. This means that only a small number of neurons are activated and the computational complexity is greatly reduced.

$$i_C^j = f\left(I_{input} * W_C^j + b\right), \tag{12}$$

$$f(x) = \max(0, x), \tag{13}$$

where $f(x)$ is the activation function, which is used to nonlinear the data after the convolution operation; * is the convolution operation; i_C^j is the jth feature of the preprocessed current generated by the convolution kernel W_C^j map; $j \in [1, n_c]$, where n_c is the number of convolution kernels; and b is the bias. The convolution kernel $W_C^j \in R^{m\times d}$ is a weight matrix, where m is the size of the convolution kernel.

(2) Pooling layer

In practical applications, the maximum pooling method is often used. This method extracts the local maximum from the input features, which can reduce the parameters and calculation of the next layer while retaining the main features so as to prevent overfitting. The formula is as follows:

$$x_m^{pout} = \max\left(x^{pin} e\sigma_m\right), \tag{14}$$

where x^{pin} is the input data of the pooling layer, σ_m is the coverage of the filter of this layer in the mth step of sliding on x^{pin}, and $\odot$ is the value taken.

(3) Fully connected layer

The fully connected layer contains multiple hidden layers that abstractly combine the timing features of the current signal after global preprocessing. The SoftMax classifier is used to determine the failures after fully connected layers. The calculation formula of the fully connected layer is as follows:

$$x_j^l = f\left(\sum W_{ij}^l x_i^{l-1} + b_j^l\right), \tag{15}$$

where x_i^{l-1} is the output of the ith neuron in the l-1th layer, x_j^l is the output of the jth neuron in the lth layer after the fully connected layer, W_{ij}^l is the weight matrix, b_j^l is the bias, and f is the activation function.

3 Dataset and implementation details

3.1 Experimental setup

Based on the GB14287.4-2014 [21] and UL1699-2011 standards [22], we built a series arc fault test platform. A low power current transformer with a bandwidth of 200 kHz was used as the current transformer, and a voltage transformer was used to collect the voltage across the arc simulator to distinguish between the normal and fault currents. The arc fault simulator comprises a graphite electrode with a diameter of 6 mm as a static contact and a copper electrode with a diameter of 6 mm as a moving contact. By turning the knob of the arc simulator, a very small gap is generated between the electrodes, and the voltage between the electrodes breaks down the gap, resulting in an arc. The actual experimental platform is shown in Figure 2.

In this work, five loads were used as experimental objects: a heater, an induction cooker, a computer, a microwave oven, and a vacuum cleaner. The current data was collected using an oscilloscope. The used sampling frequency was 50 kHz to entirely acquire the cycle signal data. 1500 groups of current signals before and after five kinds of load faults were collected, respectively, with a total of 15,000 groups of data.

Figure 3 shows a comparison of the current waveforms before and after the five types of load faults. Each waveform started to fail when the time.

3.2 Characteristics of the series arc

As shown in Figure 3, the normal load current waveform of the heater is a regular sine wave, while the normal load

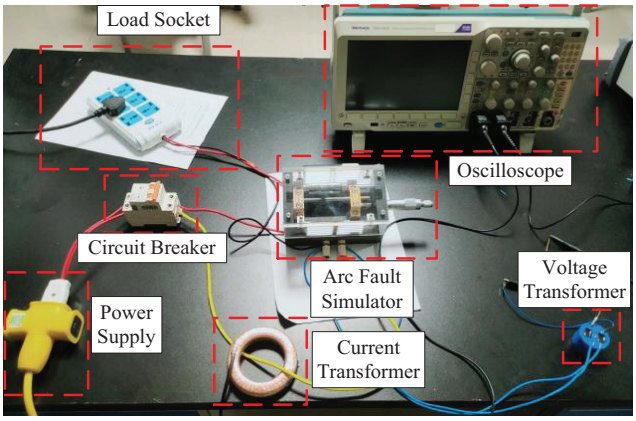

Fig. 2. Actual experimental platform.

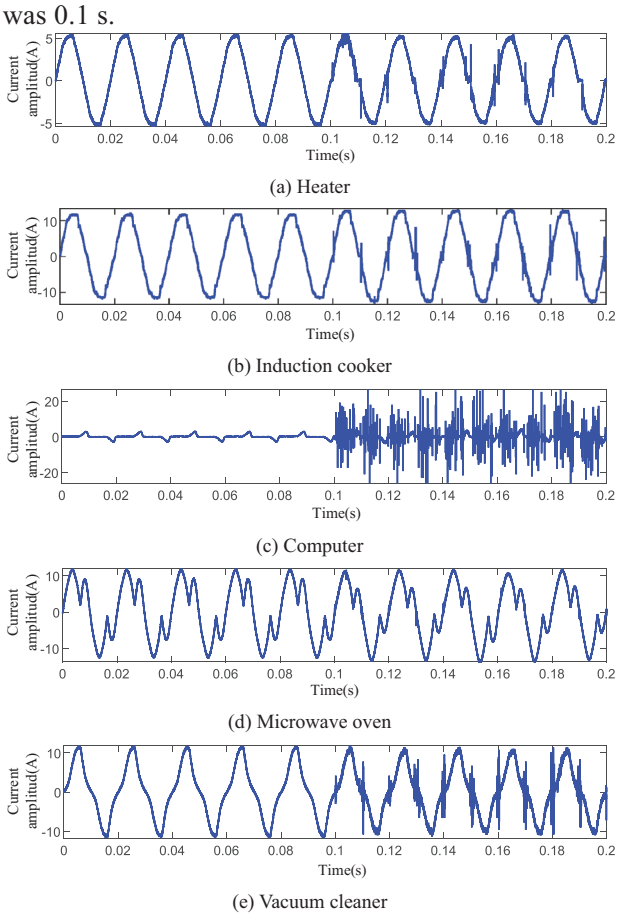

Fig. 3. Comparison of current waveforms before and after different load faults.

current waveform of the induction cooker has a small number of harmonic components. The fault current waveforms of the two types of loads both show obvious zero-break characteristics. The normal load current waveform itself of the computer has obvious zero-break characteristics. On this basis, the fault current waveform has a large number of high-frequency burrs. The normal load current waveform of the microwave oven has two peaks in one half-wave, and the fault current waveform has

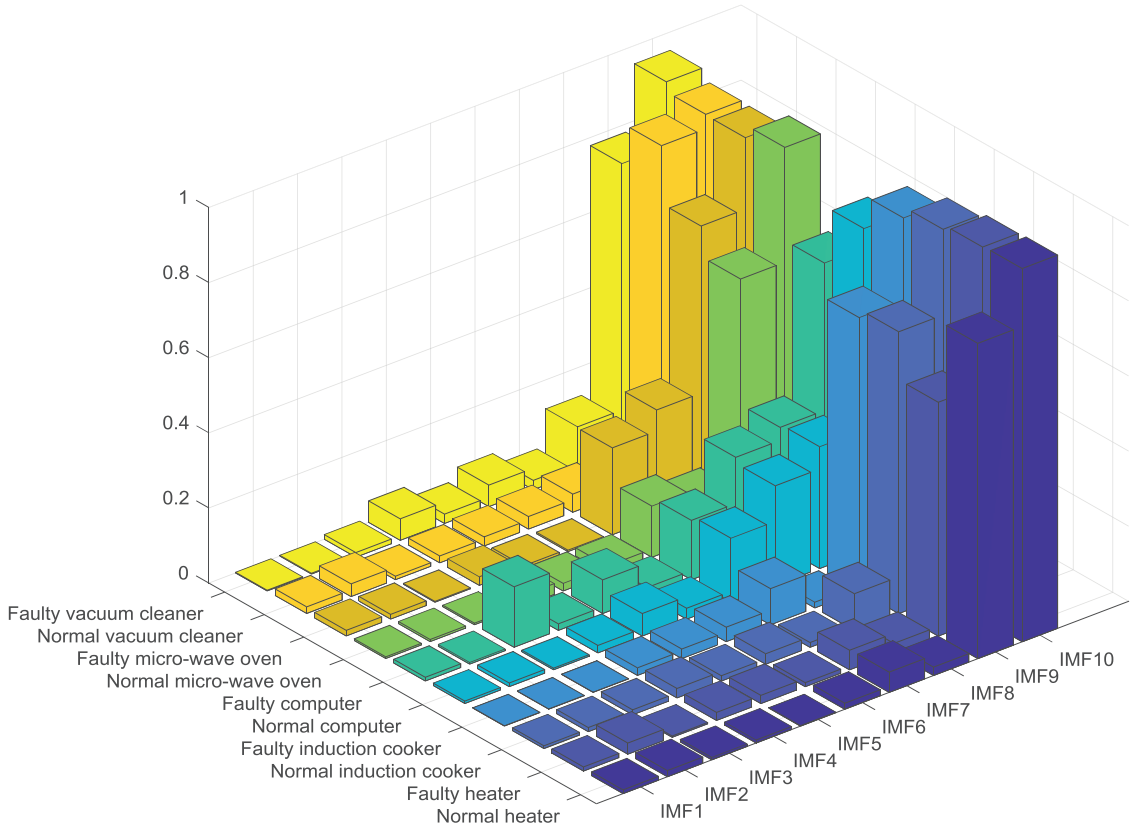

Fig. 4. Absolute value of Spearman correlation coefficients of each IMF component and standard power frequency sinusoidal current signal.

no zero-break characteristics. The burr phenomenon is not obvious, and only the time-domain waveform distortion phenomenon in which the amplitude of the second peak is one half-wave was reduced. The normal load current waveform of the vacuum cleaner is approximately a triangular wave, and the fault current waveform does not have zero-break characteristics, where only the high-frequency burrs appear at the zero-crossing point of the current. Overall, it can be seen that it is difficult to use a unified criterion to detect series arc faults.

3.3 Data pretreatment of test

Each full cycle signal with 1000 data points was used as a test object. After the original current signal was collected at the sampling rate of 50 kHz, the CEEMDAN algorithm was used to decompose the raw current signals. The current signals of the five loads before and after the fault were decomposed into IMF components comprising 9–13 layers, where most of them were decomposed into 10 or 11 layers, and a few were decomposed into 9, 12, or 13 layers.

According to the Spearman correlation coefficient between the IMF component and standard power frequency sinusoidal current for the typical decomposition case shown in Figure 4, among the IMF, the correlation coefficients of IMF1, IMF2, IMF3, IMF4, IMF5, IMF6, IMF7, and IMF8 are effective IMF components.

This research connects the effective IMF components in series as samples of the CNN model. After effective IMFs were reconstructed as CNN input samples, effective features could be located at different locations of the samples. Each position of the sample could be scanned by the same convolution kernel, and the weights in the convolution kernel were not changed as the convolution kernel moved, thus realizing weight sharing. The premise of weight sharing is that in a sample, each data point is only related to the surrounding data points. When data is reconstructed into a two-dimensional matrix, the data points between the two rows lack correlation. Thus, this research reconstructed the data as a 1D matrix, and classification was implemented using a 1D convolutional neural network.

3.4 Evaluation metrics

For different models, evaluation metrics need to be used for comparison purposes. Accuracy refers to the proportion of the correctly identified samples among all samples, precision refers to the proportion of the true positive samples among the samples predicted to be positive, recall refers to the proportion of the samples predicted to be positive among the true positive samples, and F-1 reflects the model robustness. In the identification of series arc faults, the false alarm rate and missing alarm rate are the main focus of attention. The false alarm rate indicates the proportion of the real normal

samples that are predicted to be faults, and the missing alarm rate indicates the real fault samples predicted to be normal. The mathematical expression of the abovementioned evaluation indicators is as follows:

$$\begin{cases} f_{accuracy} = \dfrac{TP + TN}{TP + TN + FP + FN} \\ f_{precision} = \dfrac{TP}{TP + FP} \\ f_{recall} = \dfrac{TP}{TP + FN} \\ F - 1 = \dfrac{2 * f_{precision} * f_{recall}}{f_{precision} + f_{recall}} \\ f_{far} = \dfrac{FN}{TP + FN} \\ f_{mar} = \dfrac{FP}{TN + FP} \end{cases}, \tag{16}$$

where $f_{accuracy}$ is the accuracy rate, $f_{precision}$ is the precision rate, f_{recall} is the recall rate, f_{far} is the false alarm rate, f_{mar} is the missing alarm rate, TP (true positive) is the number of samples that correctly predict the positive class as a positive class, TN (true negative) is the number of samples that correctly predict a negative class as a negative class, FP (false positive) is the number of samples that incorrectly predict a negative class as a positive class, and FN (false negative) is the number of samples that incorrectly predict a positive class as a negative class.

4 Experimental results

4.1 CNN training

The structure and parameter settings of the CNN model have an important impact on the accuracy and efficiency of fault diagnosis. To identify the optimal model parameters, in this research, 1DCNN topologies were designed with different structures, and experiments were conducted.

For each model, the convolution kernel and pooling kernel have the same size, the stride of the convolution kernel is 1, and the stride of the pooling kernel is the same as the kernel length. Each convolutional layer is followed by a pooling layer. The kernel size, number of kernels, and structure settings of the hidden layers of different models are shown in Table 1. Taking the No. 1 model as an example, the kernel size of the convolutional layer and the pooling layer of this model are both 1×5, and the structure of the hidden layer is a convolutional layer with four convolutional kernels followed by a pooling layer.

The adaptive moment estimation (Adam) gradient optimization algorithm was used for optimization. Generally, this method has the advantages of AdaGrad and RMSProp, improves the gradient calculation method and learning rate, and optimizes the problems of gradient oscillation and slow optimization speed.

In this work, 12,000 training samples and 3000 test samples were selected, and the same train and test sets were used by each CNN model. The number of iterations set by the CNN was 50, and the minibatch size was set to 27. Table 2 shows experimental results of each CNN model.

Table 1. Structural parameters of CNN model.

No.	Kernel size	Structural
1	1×5	4-4
2	1×5	4-4-8-8
3	1×5	4-4-8-8-16-16
4	1×3	4-4
5	1×3	4-4-8-8
6	1×3	4-4-8-8-16-16
7	1×5	2-2-10-10
8	1×5	2-2-5-5-10-10
9	1×3	2-2-10-10
10	1×3	2-2-5-5-10-10

Each model was trained ten times, and the obtained results were averaged. The test time refers to the time taken to test all the 3000 test samples. Overall, the results show that under the same other conditions, the model with a kernel size of 1×5 has higher recognition accuracy with regard to the test set than the model with a kernel size of 1×3, although the model with the deeper hidden layers took longer to train. Nevertheless, the precision also tended to be higher. According to the comparison of the experimental results in Table 2, the recognition accuracy of the No. 3 model with regard to the test set was highest, 99.3%, and the test time was shortest, 0.687 s. The average test time per sample was 0.229 ms. Therefore, NO.3 was selected as the CNN model parameter setting.

4.2 Pretreatment comparison test

In order to further verify the effectiveness of the proposed data preprocessing method, this research use the dataset consisting of the raw current signal, the dataset consisting of the IMF components after processing the original current signal by the EMD decomposition algorithm and the dataset consisting of the IMF components after processing the original current signal by the EEMD decomposition algorithm as the input of CNN for comparative experiments. Figure 5 shows the relationship between the training set accuracy of different models and the number of iterations. Figure 6 shows the recognition results of different models on the running state in the test set. 1DCNN model is a model that uses the raw current signal as the CNN input.

As shown in Figure 6, the accuracy of the 1DCNN model is significantly lower than the other three models that preprocess the raw current signal. The 1DCNN model tends to identify normal samples as faulty samples with a high false alarm rate. The accuracy of the EMD-1DCNN model is lower than that of the EEMD-1DCNN model and the CEEMDAN-1DCNN model due to the presence of modal aliasing in EMD. Compared with other recognition models, the model using CEEMDAN decomposition and 1DCNN has the fastest convergence speed, and has the highest accuracy, precision, recall and F-1 score, while the false alarm rate and the false alarm rate are the lowest.

Table 2. Experimental results of different models.

No.	Average training time/s	Average test accuracy/%	Average test time/s
1	279	87.8	0.724
2	328	94.3	0.714
3	387	99.3	0.687
4	297	87.0	0.802
5	322	89.4	0.749
6	321	95.6	0.937
7	341	95.5	0.876
8	406	96.2	0.705
9	339	90.6	0.774
10	411	90.2	0.815

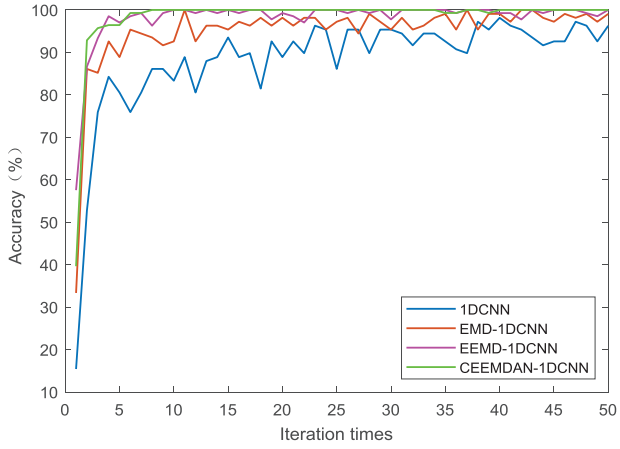

Fig. 5. Training set accuracy curves of different models.

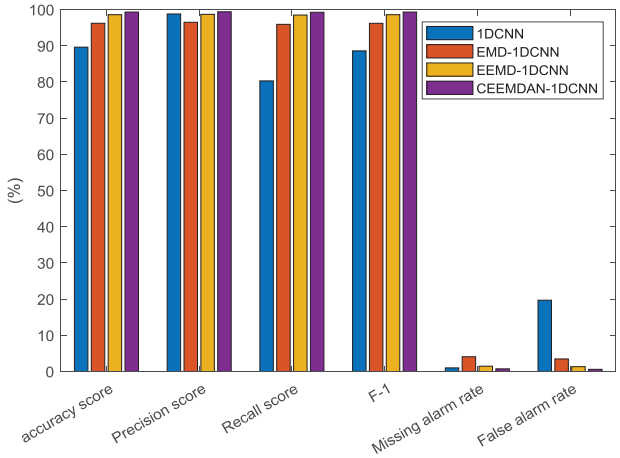

Fig. 6. Identification results of different models on test sets.

5 Conclusion

In this paper, a series arc fault detection model based on CEEMDAN-1DCNN is proposed. An experimental platform was built to collect the current data of five load normal and fault states and then perform tests. The main conclusions are as follows.

– Using the IMF components of the current signal decomposed by the CEEMDAN algorithm to construct training samples can efficiently reflect the fault information of CNNs and also improve their training speed and recognition accuracy.
– As deep learning methods, CNNs can mine data features and learn independently. Thus, they have strong intelligence, and the uncertainty caused by traditional manual feature extraction methods can be avoided.

Although measures have been taken to reduce the size of CNN input data, there are still certain requirements regarding the computing power of the used equipment. Therefore, the next research focus should be to further simplify the number of IMFs and select a suitable microprocessor for realizing the hardware implementation of the arc fault detection algorithm.

Funding Information

This work is supported by National Science Foundation of China (Grant No. 52077221).

Author contribution statement

Tongtong Shang: Methodology, Software, Data Curation, Writing - Original Draft. Wei Wang: Conceptualization, Resources, Writing - Review & Editing, Supervision. Jigang Peng: Writing - Review & Editing, Visualization. Bingyin Xu: Project administration, Funding acquisition. Haiyang Gao: Investigation. Guoliang Zhai: Validation.

References

1. T. Crnko, S. Dyrnes, Arcing fault hazards and safety suggestions for design and maintenance, IEEE Ind. Appl. Mag. **3**, 23–32 (2001)
2. J.H. Du, R. Tu, Y. Zeng, L. Pan, R.C. Zhang, An experimental study on the thermal characteristics and heating effect of arc-fault from Cu core in residential electrical wiring fires, PLoS ONE **12**, e0182811 (2017)

3. Y. Liu, J. Zheng, L. Li, Analysis of characteristics of fault arc in series under influence of ambient humidity, Proc. CSU-EPSA **08**, 7–12 (2019)
4. J.P. Pulkkinen, Commercial arc fault detection devices in military electromagnetic environment, IEEE Electromagn. Compat. Mag. **4**, 49–52 (2018)
5. Q. Lu, Z. Ye, Y. Zhang, T. Wang, Z. Gao, Analysis of the effects of arc volt-ampere characteristics on different loads and detection methods of series arc faults, Energies **12**, 323 (2019)
6. X. Qin, Y. Liu, P. Sun, Study on the line fault root-cause identification method in distribution networks based on time-frequency characteristics of fault waveforms, Chinese J. Sci. Instrum. **1**, 41–49 (2017)
7. G. Artale, A. Cataliotti, V. Cosentino, D. Di Cara, S. Nuccio, G. Tinè, Arc fault detection method based on CZT low-frequency harmonic current analysis, IEEE Trans. Instrum. Measur. **5**, 888–896 (2017)
8. Y. Abdullah, B. Hu, Z. Wei, J. Wang, A. Emrani, Adaptive detection of DC Arc faults based on hurst exponents and current envelope, IEEE Appl. Power Electr. Conf. Exposition (APEC), 3392–3397 (2018)
9. H. Zhao, J. Liu, J. Lou, Series arc fault detection based on current fluctuation and zero-current features, Electr. Power Syst. Res. **202**, 107626 (2022)
10. K. Yang, R. Zhang, S. Chen, F. Zhang, J. Yang, X. Zhang, Series arc fault detection algorithm based on autoregressive bispectrum analysis, Algorithms **8**, 929–950 (2015)
11. S.B. Lu, B.T. Phung, D.M. Zhang, A comprehensive review on DC arc faults and their diagnosis methods in photovoltaic systems, Renew. Sustain. Energy Rev. **89**, 88–98 (2018)
12. Q. Yu, G. Huang, Y. Yang, Y. Sun, Series arc fault detection method based on AlexNet deep learning network, J. Electr. Meas. Instrum. **03**, 145–152 (2019)
13. Z. Jiao, T. Li, L. Wang, L. Mou, A. Khalyasmaa, Dc series arc fault detection of photovoltaic system based on convolution neural network, Adv. Technol. Electr. Eng. Energy. **07**, 29–34 (2019)
14. Y. Wang, F. Zhang, S. Zhang, A new methodology for identifying arc fault by sparse representation and neural network, IEEE Trans. Instrum. Meas. **11**, 2526–2537 (2018)
15. K. Yang, R. Chu, R. Zhang, J. Xiao, R. Tu, A novel methodology for series arc fault detection by temporal domain visualization and convolutional neural network, Sensors **1**, 162 (2020)
16. Q. Yu, Y. Hu, Y. Yang, Identification method for series arc faults based on wavelet transform and deep neural network, Energies **13**, 142 (2020)
17. Y. Wang, F. Zhang, S. Zhang, G. Yang, A novel diagnostic algorithm for AC series arcing based on correlation analysis of high-frequency component of wavelet, COMPEL. **1**, 271–288 (2017)
18. M.E. Torres, M.A. Colominas, G. Schlotthauer, P. Flandrin, A complete ensemble empirical mode decomposition with adaptive noise, in *IEEE International Conference on Acoustics, Speech and Signal Processing (ICASSP)* (2011) pp. 4144–4147
19. W.-Y. Zhang, Z.-W. Wei, B.-H. Wang, X.-P. Han, Measuring mixing patterns in complex networks by Spearman rank correlation coefficient, Physica A **451**, 440–450 (2016)
20. D.E. Rumelhart, G.E. Hinton, R.J. Williams, Learning representations by back-propagating errors, Nature **323**, 533–53 (1986)
21. General Administration of Quality Supervision, Inspection and Quarantine of the People's Republic of China: Electrical Fire Monitoring System-Part 4: Arcing Fault Detectors (GB 1428 7.4-2014) (Standards Press of China: Beijing, China, 2014)
22. Underwriters Laboratories Inc., UL Standard for Arc-Fault Circuit-Interrupters, 2nd edn., (Underwriters Laboratories Inc.: New York, NY, 2011)

Cite this article as: Tongtong Shang, Wei Wang, Jigang Peng, Bingyin Xu, Haiyang Gao, Guoliang Zhai, Series arc fault identification based on complete ensemble empirical mode decomposition with adaptive noise and convolutional neural network, Int. J. Metrol. Qual. Eng. **13**, 11 (2022)